Delft University of Technology

Smart aggregates for acoustic emission monitoring of concrete cracking and reinforcement corrosion

Van Steen, Charlotte; Pahlavan, Lotfollah; Verstrynge, Els

DOI
10.1016/j.conbuildmat.2024.137644

Publication date
2024

Document Version
Final published version

Published in
Construction and Building Materials

Citation (APA)
Van Steen, C., Pahlavan, L., & Verstrynge, E. (2024). Smart aggregates for acoustic emission monitoring of concrete cracking and reinforcement corrosion. *Construction and Building Materials*, *443*, Article 137644. https://doi.org/10.1016/j.conbuildmat.2024.137644

Important note
To cite this publication, please use the final published version (if applicable).
Please check the document version above.

Copyright
Other than for strictly personal use, it is not permitted to download, forward or distribute the text or part of it, without the consent of the author(s) and/or copyright holder(s), unless the work is under an open content license such as Creative Commons.

Takedown policy
Please contact us and provide details if you believe this document breaches copyrights.
We will remove access to the work immediately and investigate your claim.

This work is downloaded from Delft University of Technology.
For technical reasons the number of authors shown on this cover page is limited to a maximum of 10.

Green Open Access added to TU Delft Institutional Repository

'You share, we take care!' - Taverne project

https://www.openaccess.nl/en/you-share-we-take-care

Otherwise as indicated in the copyright section: the publisher is the copyright holder of this work and the author uses the Dutch legislation to make this work public.

Construction and Building Materials 443 (2024) 137644

Contents lists available at ScienceDirect

Construction and Building Materials

journal homepage: www.elsevier.com/locate/conbuildmat

Smart aggregates for acoustic emission monitoring of concrete cracking and reinforcement corrosion

Charlotte Van Steen [a,*], Lotfollah Pahlavan [b], Els Verstrynge [a]

[a] Department of Civil Engineering, KU Leuven, Belgium
[b] Maritime and Transport Technology, Delft University of Technology, the Netherlands

ARTICLE INFO

Keywords:
Acoustic emission
Embedded sensor
Smart aggregate
Cracking
Reinforcement corrosion
Reinforced concrete

ABSTRACT

The acoustic emission (AE) technique allows monitoring damage in (reinforced) concrete in a non-destructive way by means of piezoelectric sensors attached to the material surface. This approach has disadvantages such as a decrease of the sensor coupling over time, high attenuation of AE waves in concrete, and difficulties in terms of sensor placement. Embedded AE sensors, so-called 'smart aggregates' (SA), can be a valuable addition or alternative to surface-mounted AE sensors. However, the embedment of sensors brings its own challenges. In this paper, the use of SA is investigated to monitor cracking of fiber reinforced concrete during a three-point bending test, and corrosion and related concrete cracking of reinforced concrete during an accelerated corrosion test. The novelty of the paper is the application of SA for passive AE monitoring during concrete degradation processes with a varying cracking behavior and crack orientation. Special emphasis is put on data filtering and localization of AE sources. The results show that, despite a higher level of wide-band noise for the SA sensors, they are able to detect and localize concrete cracking after dedicated filtering. Furthermore, the potential of SA sensors in early-stage detection of corrosion damage is demonstrated, offering enhanced possibilities for predictive maintenance of concrete structures.

1. Introduction

The acoustic emission (AE) technique is a non-destructive monitoring technique which allows to continuously monitor the damage evolution in various materials [1–4], among which brittle materials such as reinforced and fiber reinforced concrete (RC and FRC) [5–7]. The AE technique detects high-frequency elastic waves being produced by the damage process itself, which is why it is referred to as a passive technique. In current practice, piezoelectric or fiber-optic AE sensors are attached on the surface of the structural component. The AE technique has been extensively used in laboratory testing to detect cracking in concrete due to mechanical loading such as three- and four-point bending tests [6,8,9] and pull-out tests [10–12], or due to deterioration phenomena such as corrosion [13–16] and alkali-silica reaction (ASR) [17,18].

The AE technique has many advantages. It allows to detect, locate, and characterize damage from an early stage in the damage process. However, attaching the sensor on the surface requires attention in terms of placement and coupling of the sensors. A stable coupling between sensor and structure is difficult to maintain over time. Therefore, the measurement accuracy may decrease in long-term monitoring applications. Moreover, due to the high attenuation properties of concrete, the AE signal strength may drop below the detection threshold before reaching the sensor. In addition, it is not always possible to attach sensors in harsh and/or hazardous environments, or structures with limited access.

Embedded sensors or "smart aggregates (SA)" can be used as an alternative in order to avoid externally mounted sensors. In this way, an aggregate-mimicking AE sensor, typically consisting of a piezoelectric patch in a mortar or stone case, is embedded in the concrete while casting or, in case of an existing structure, inserted at the location where a core was drilled before refilling of the void. Although important disadvantages of externally mounted AE sensors may be overcome, the use of SA brings its own challenges. The piezoelectric patch is fragile and susceptible to external pressure or force. The case that protects the piezoelectric patch may have an impact on the AE signal and on the mechanical behavior of the structure in which the SA sensors are embedded. Moreover, the monitoring range of SA may be limited as most patches are two-dimensional [19].

In case of elastic wave methods, it should be noted that SA can be

* Corresponding author.
E-mail address: charlotte.vansteen@kuleuven.be (C. Van Steen).

https://doi.org/10.1016/j.conbuildmat.2024.137644
Received 14 March 2024; Received in revised form 24 June 2024; Accepted 25 July 2024
Available online 2 August 2024
0950-0618/© 2024 Elsevier Ltd. All rights reserved, including those for text and data mining, AI training, and similar technologies.

used as passive sensors or as active transducers. Transducers can sense and actuate while a sensor can only sense [20]. Most SA are applied to actively send ultrasonic waves using the principle of ultrasonic pulse velocity (UPV) measurements and are therefore transducers. This means that one SA, the transmitter, sends ultrasonic pulses to other SA, the receivers. The obtained wave velocity is a measure for the damage state of the concrete within the travel path of the wave.

In the current state of the art, research on SA detecting elastic waves is still limited and they are mainly applied as transducers. In concrete, SA were used as transducers to monitor early-age strength [21,22], the seismic behavior of concrete columns [23] and crack detection of an RC beam under three-point bending [24]. For reinforcement corrosion detection, Liu et al. [25] found that the extent of corrosion could be qualitatively evaluated by variations in acoustic energy and the dominant frequency component of the ultrasonic wave. Peak-peak values as well as the peak of the dominant frequency tend to decrease over time when corrosion progresses. Moreover, new peaks at lower frequencies can be observed.

When looking at research on SA as passive sensors, Li et al. [26] used SA sensors as an alternative to AE sensors during three-point bending tests of prisms in plain concrete. It was found that the AE parameters, such as hits, amplitude and counts, from both the SA sensors and traditional AE sensors showed similar characteristics. We refer to AE standards and guidelines for typical AE terminology [20,27]. Lu et al. [28] used embedded sensors during dry-wet tests to evoke reinforcement corrosion. Two beams undergoing corrosion and loading were investigated as well as two corroding beams without loading. The onset of concrete corrosion and concrete cracking was identified. However, no comparison with surface-mounted sensors was made.

From this literature overview, it can be seen that the feasibility of using SA as sensors for passive AE monitoring, meaning that signals originate from the damage process such as concrete cracking itself, is much less investigated. The aim of this paper is to investigate whether SA sensors can be used as an alternative or as an addition to classic surface-mounted AE sensors to monitor corrosion and cracking in (F)RC during degradation.

In this paper, cracking in representative concrete specimens will be induced by mechanical loading (i.e., three-point bending test) and by reinforcement corrosion, leading to a different cracking behavior and crack orientation. The main novelty of the paper is the application of SA sensors for crack detection in (F)RC using passive AE monitoring. Special emphasis is put on AE signal filtering and localization in order to compare their behavior and sensitivity with surface-mounted AE sensors. Especially the application of SA sensors combined with surface-mounted AE sensors for corrosion damage detection extends beyond the current state of the art.

2. Working principle and characteristics of the embedded sensors

The SA sensors applied in this research are piezoelectric patches embedded in high-strength mortar for protecting the sensor patch while ensuring optimum acoustic impedance matching with the host concrete material when measuring AE signals. While the general transduction mechanism of piezoelectric materials holds for SA sensors in measuring strain and AE signals, the dimensions, directionality, and embedment details of the piezoelectric transducer additionally influence their transfer function and sensitivity. Proper design and selection of SA sensors is hence of importance per application. In this research, SA sensors of type ‘Agent’ by SHM NEXT are used for measuring AE signals inside concrete specimens. These embedded SA are spherical, have an outer diameter of 35 mm and offer a wide-band response below 150 kHz. Fig. 1 shows a picture and a schematic representation of two cross sections of the SA sensor.

The sensitivity and directionality of each SA sensor was studied by performing pencil lead breaks PLB) on the SA sensors before embedment. Fig. 2 shows the result of these PLB which were done at mid-height around the perimeter of the SA sensor. An indication is given on the position of the piezoelectric patch. Relative results are presented meaning that the peak amplitude of each AE signal at each point was divided by the maximum peak amplitude found at the respective SA sensor. The sensors tend to be the least sensitive at point 7. The maximum relative difference between the most sensitive point and this point is found to be 0.13, which can be considered as a minor reduction. Overall, the results are consistent and the sensors perform well omnidirectional.

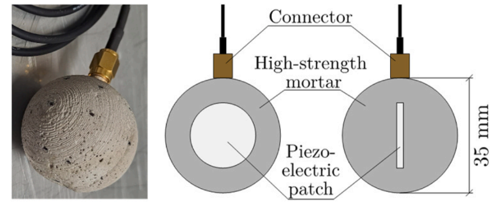

Fig. 1. Picture (left) and schematic representation of two cross sections (right) of the SA sensor.

Fig. 3 shows a typical AE signal in the frequency domain obtained from a PLB performed at point 5. The digital frequency filter of the AE acquisition system was chosen between 25 and 850 kHz. It can be seen that the sensors are most sensitive below 150 kHz with peaks around 49, 79, 109 and 125 kHz. Other point and sensors show similar characteristics.

3. Experimental test program: three-point bending tests

3.1. Materials and specimen preparation

The applied setup and materials are based on previous work performed on AE monitoring of FRC [6]. Three FRC prisms having dimensions 150x150x660 mm were cast in accordance with European Standard EN 14651 [29]. The concrete composition is shown in Table 1 and is identical for all specimens. The mean cube compressive strength was 59 MPa (standard deviation 2.8 MPa) as tested on three cubes at 28 days according to EN 12390-3 [30]. Dramix3D-80/60-BG steel fibers with a dosage of 20 kg/m^3 were used.

In two of the three prisms (prism 1 and prism 3), the SA were placed in the formwork before concrete casting. To hold the SA in place, steel wires which were fixed to the formwork, were used as shown in Fig. 4. After casting, the specimens were placed in a curing chamber with a constant temperature of 20 $\pm$ 5 °C and relative humidity of 95 $\pm$ 3 %.

In prism 2, the SA were placed after curing by drilling a core with a diameter of 52 mm and filling this void with mortar. Core drilling and testing is a common practice for the assessment of the concrete strength in existing buildings. The composition of the filling mortar is shown in Table 2. The mortar had a mean compressive strength of 53 MPa (standard deviation 2.0 MPa) at 28 days as tested following EN 196-1 [31].

A front and top view of the sensor placement for each prism are shown in Fig. 5. In all prisms, the SA sensors were positioned on one line in the middle of the height of the sample. In prism 1, two SA sensors are placed on a horizontal line along the length of the sample with a distance of 250 mm in between. The piezoelectric patch faces towards the other SA sensor. In prism 2, the SA sensors are positioned in the same layout. In prism 3, only one SA was placed at middle height close to the back of the sample. For each sample, two standard AE sensors are positioned on the sample surface, as indicated in Fig. 5. As they are mounted on the surface, they are mostly one-directional as indicated, while the SA sensors have the highest sensitivity in the direction perpendicular to the sensor patch, see Fig. 5. Details of AE sensors and acquisition setup are discussed in Section 3.3.

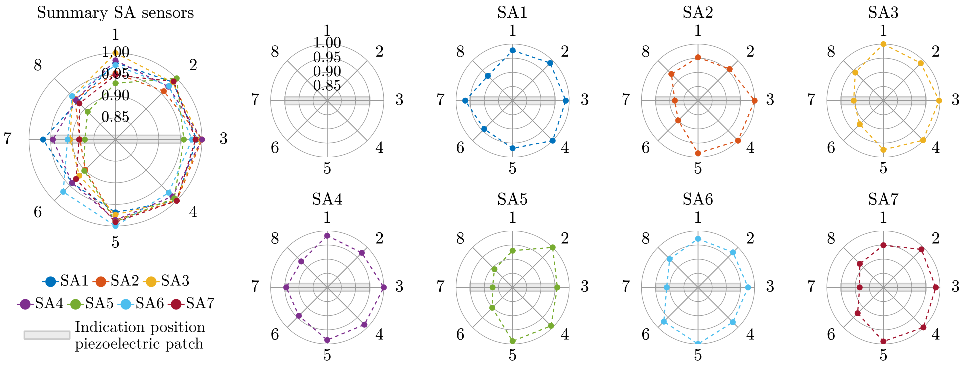

Fig. 2. Study of the sensitivity and directionality of the SA sensors with indication of the position of the piezoelectric patch.

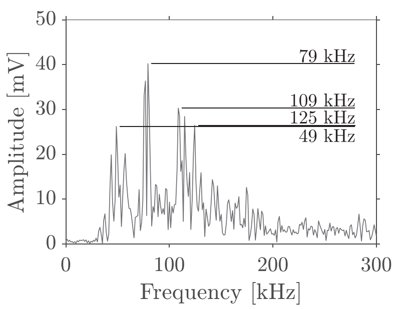

Fig. 3. AE signal in the frequency domain obtained from a pencil lead break on the SA sensor before embedment.

Table 1
Concrete composition for the samples tested under three-point bending.

Material	kg/m^3
CEM I 52.5 N	350
Sand 0/4	835
Gravel 4/14	1099
Water	175
Superplasticizer Glenium 51	1
Dramix 3D−80/60-BG	20

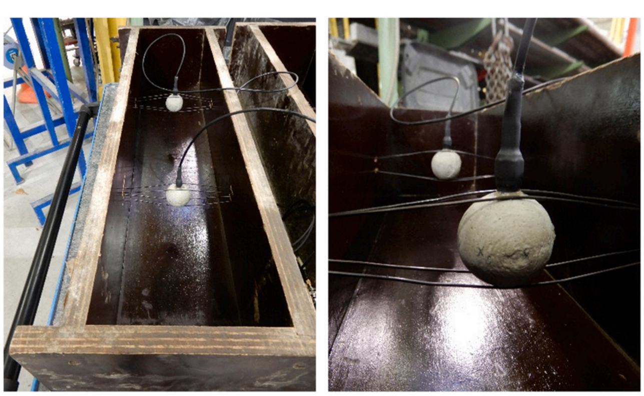

Fig. 4. Pictures of the formwork for the three-point bending tests with the smart aggregates held in place by steel wires fixed to the sides of the formwork.

3.2. Three-point bending test setup

The FRC prisms were subjected to a three-point bending test according to EN 14651 [29], see also Fig. 6. A hydraulic press with a maximum capacity of 5 MN was used. A notch with a height of 25 mm

Table 2
Filling mortar composition for prism 2.

Material	kg/m^3
CEM I 52.5N	470
Sand 0/4	1410
Water	235

and a width of 5 mm was sawn at the bottom of the specimens to initiate the crack location. The distance between the supports was 500 mm. A linear variable differential transformer (LVDT) measured the crack mouth opening displacement (CMOD) at the bottom of the sample. A monotonically increasing load was applied in order that the CMOD increased at a constant rate of 0.05 mm/min. When the CMOD was equal to 0.1 mm, the rate was increased to 0.2 mm/min. The test was terminated when the CMOD reached a value larger than 4 mm. The applied load was measured by an external load cell having a capacity of 100 kN. Three additional LVDTs were attached on the side of the sample at heights 35 mm, 80 mm, and 125 mm from the bottom of the sample to measure the crack length and shift in neutral axis.

3.3. Acoustic emission sensing

All specimens were continuously monitored during the three-point bending tests with the AE technique. Besides the SA sensors that were embedded in the concrete, two AE sensors were attached on the surface with vacuum grease. The sensors were positioned at the same height as the SA sensors and the horizontal distance between them was 250 mm (see Figs. 5 and 6). The coordinates of the SA and AE sensors are given in Table 3. The AE sensors were broadband sensors with a flat frequency response between 100 and 400 kHz (type AE104A, Fuji Ceramics). All sensors were connected to a preamplifier (AEP4, Vallen Systeme) with a 34 dB gain. The amplifiers were connected to a Vallen AMSY-6 data acquisition system with 4 channels.

For the SA sensors, a floating amplitude threshold was set with a minimum of 45 dB to trigger recording of the AE signal (referred to as an AE hit). For acquisition of AE hits, the pre-trigger recording time, duration discrimination time and rearm time were respectively set to 200 μs, 500 μs and 2000 μs. The sampling rate was set to 5 MHz. The length of the stored AE signals was 1638.4 μs. The digital frequency filter was set to 50–200 kHz. For the AE sensors, the threshold was set to 40 dB (fixed) and the digital frequency filter to 65–200 kHz. The other settings were similar to the SA sensors.

3.4. Results of the three-point bending tests and discussion

First of all, it was found that many noise signals were captured by the SA sensors during the three-point bending tests. An example of a noise signal is shown in Fig. 7 (top). The high noise level also has an effect on

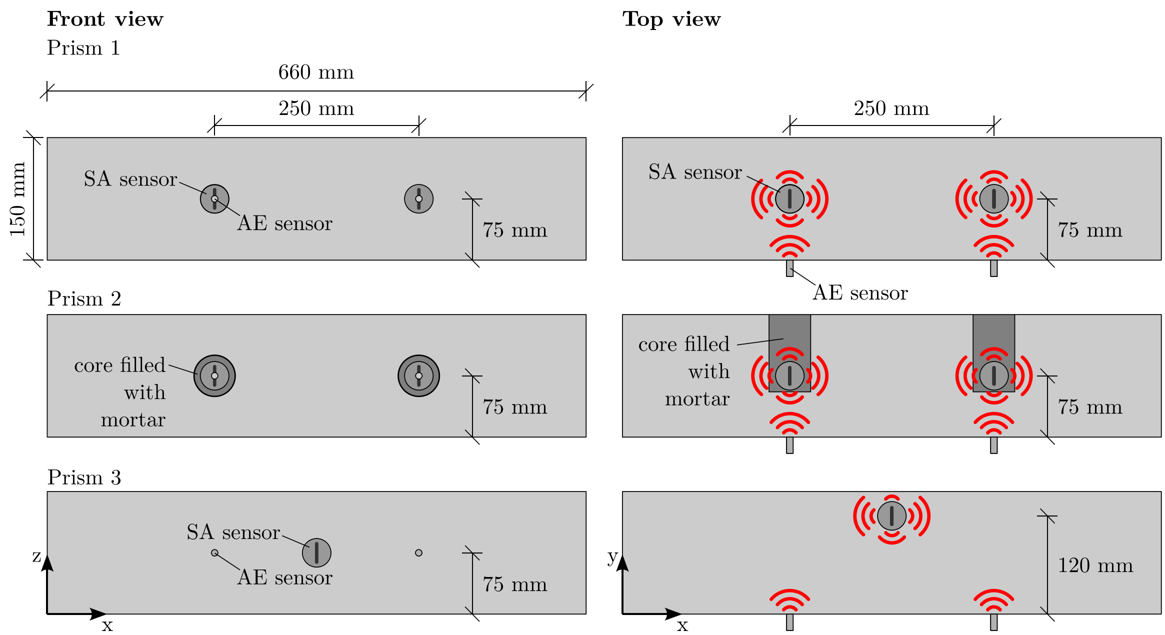

Fig. 5. Front view (left) and top view (right) of the prisms with indication of the directionality of the sensors (red).

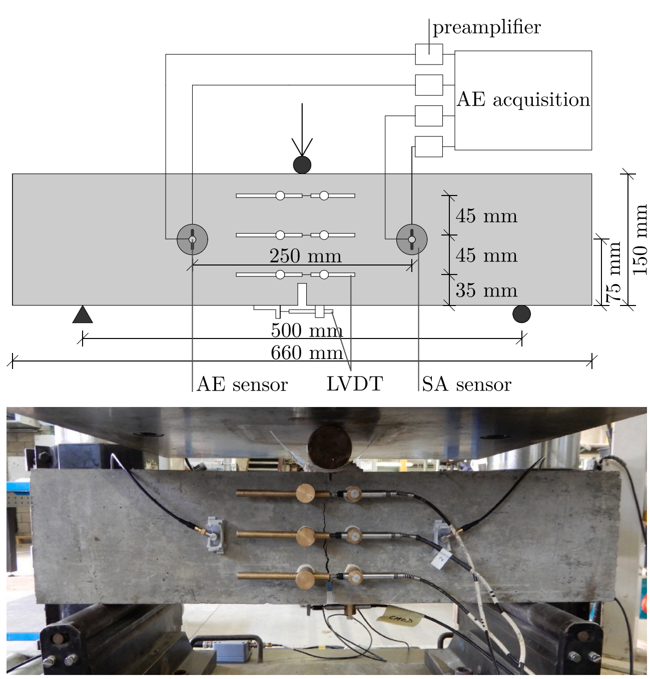

Fig. 6. Schematic representation (top) and picture (bottom) of the three-point bending test setup.

Table 3
Coordinates of the SA and AE sensors for each prism.

	X [mm]	Y [mm]	Z [mm]
Prism 1 and prism 2			
SA 1	205	75	75
SA 2	455	75	75
AE 1	205	0	75
AE 2	455	0	75
Prism 3			
SA 1	330	120	75
AE 1	205	0	75
AE 2	455	0	75

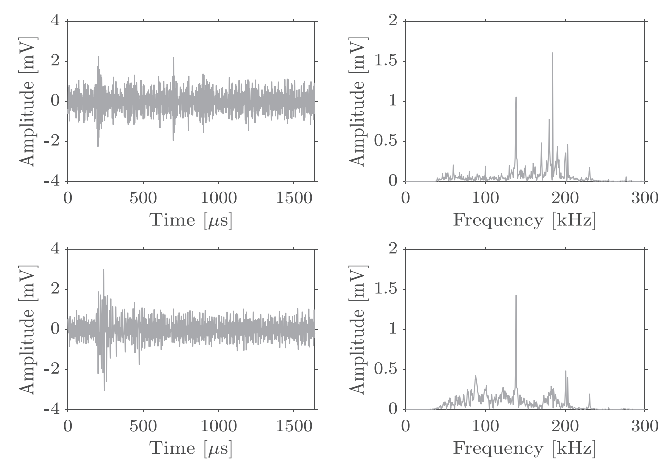

Fig. 7. Noise signal (top) and signal from concrete cracking (bottom) in time (left) and frequency (right) domain.

the detection of signals originating from concrete cracking as these signals may be masked due to the high amplitude of the noise. This can hinder accurate arrival time picking. An example of a concrete cracking signal is shown in Fig. 7 (bottom). The noise amplitude varies for the different SA sensors and is situated around 140 kHz and 180 kHz as is clear when investigating the peak frequencies of the AE signals

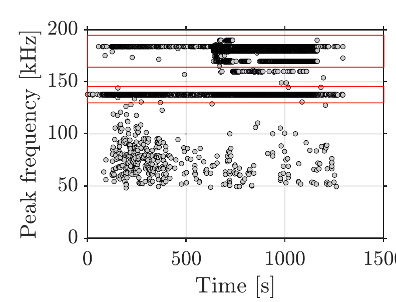

Fig. 8. Peak frequency versus time of the AE signals captured with the SA sensors. Noisy signals are clustered around 140 and 180 kHz as indicated in red.

visualized in Fig. 8. The noise may be caused by stresses from the surrounding concrete, the connection wires to hold the sensors in place, background noise, or a high sensitivity of the SA sensors.

The AE wave velocity was determined by pulsing from the AE sensors to the other sensors. This means that each AE sensor in turn emits ultrasonic pulses or bursts which are captured by the other sensors upon which the time difference is calculated. In this way, an average velocity can be obtained which is respectively 2983, 2395, and 3181 m/s for prism 1, prism 2, and prism 3. This velocity is threshold-based meaning that the first amplitude threshold crossing of an AE hit is used as arrival time of the signal. Due to the high noise level, a high threshold of 65 dB was applied for both the SA and AE sensors during calibration of the wave velocity.

To avoid overload of the AE system due to the high noise level during the three-point bending tests, a threshold-to-noise ratio (TNR) filtering was applied during acquisition for the SA. The TNR value was set at 5 for prisms 1 and 2, and at 7 for prism 3. Using a TNR filter results in a floating threshold depending on the root-mean-square (RMS) of the signal and is always equal or greater than the minimum amplitude threshold as mentioned in Section 3.3, i.e., 45 dB in case of the SA sensors. The RMS in μV is defined in the Vallen Visual AE software [32] as:

$$RMS = \sqrt{\frac{1}{T}\int_0^T U(t)^2 dt}$$

with U(t) the voltage as a function of time of the signal at sensor output [μV] and T 6.5 ms (constant).

The floating threshold, THR_{float} in dB, is defined as [32]:

$$THR_{float} = \max(THR_{\min}; 20\log(TNR \bullet RMS))$$

with THR_{min} the minimum amplitude threshold [dB], TNR the threshold-to-noise ratio [-], and RMS the root-mean-square [μV].

When applying the average threshold-based velocity found during calibration and a 1D localization algorithm with a homogeneous wave velocity, 1D localization results of the AE sensors and SA sensors can be obtained as shown in Fig. 9 for prism 1. In this figure, the extent of the cracked zone is indicated by the grey shaded area as obtained from pictures of the front and back side of the sample after testing (Fig. 10). For the AE sensors, most AE event sources are located in the middle of

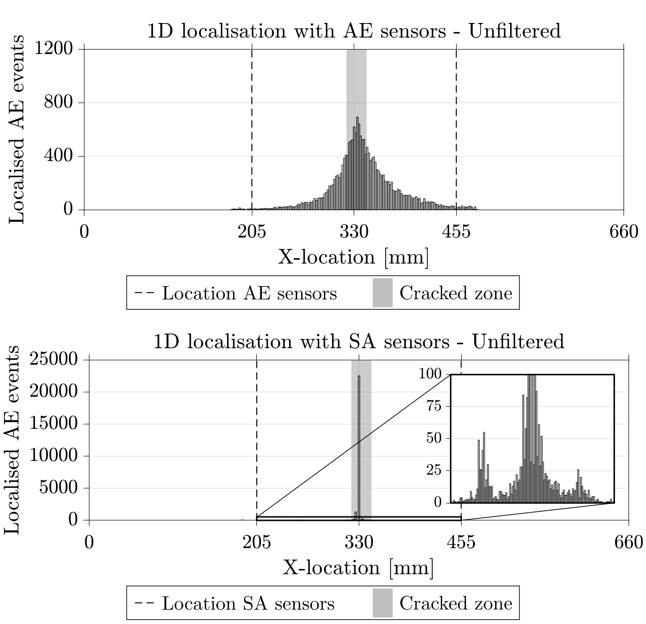

Fig. 9. 1D localization results of prism 1 using an average threshold-based velocity, obtained with the AE sensors (top) and SA sensors (bottom).

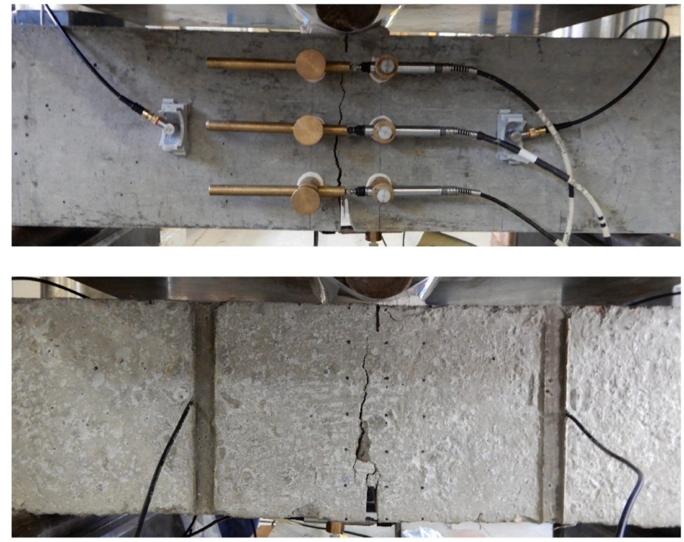

Fig. 10. Pictures of the cracked sample (prism 1) after three-point bending test, front side (top) and back side (bottom).

the specimen, as expected. The result of the SA sensors shows that many events are localized exactly in the middle of the sample. This group of AE events is considered as noise, as they would have arrived at both SA at exactly the same moment, which is unlikely due to heterogeneity of the travel path and non-perfectly symmetric cracking of the prism.

Subsequently, 2D localization was performed using both types of sensors, the surface-mounted and the embedded sensors. Geiger's algorithm assuming a homogeneous wave velocity was applied [33]. The 2D localization result of prism 1 is shown in Fig. 11. The figure shows a top view of the sample with indication of the location of the sensors and cracked zone. It can be seen that many events are localized at the front of the sample. However, a more distributed localization result along the crack length, i.e., depth of the sample or y-axis, would be expected. Remark that this result is also influenced by the sensor placement, i.e., there are no AE sensors positioned at the back of the sample. Hence, AE events in this zone are located outside the region of interest that is defined by the SA and AE sensors.

From the above analysis, it is clear that the high noise level causes many unwanted signals to be captured. It also results in a high threshold, an inaccurate arrival time determination and uncertain wave velocity value. In order to improve the localization results, the AE signals were filtered and arrival time picking was improved. For the signals captured by the SA sensors, firstly a lowpass Butterworth filter of order 5 with a cut-off frequency of 100 kHz was applied to reduce the noise level. The same signals as in Fig. 7 are shown in Fig. 12 after applying the lowpass Butterworth filter. This filter allows to remove the noise signals as they will have a lower amplitude after filtering, as well as reducing the noise level in the actual AE signals originating from concrete cracking. Secondly, the signals were selected based on their signal-to-noise ratio

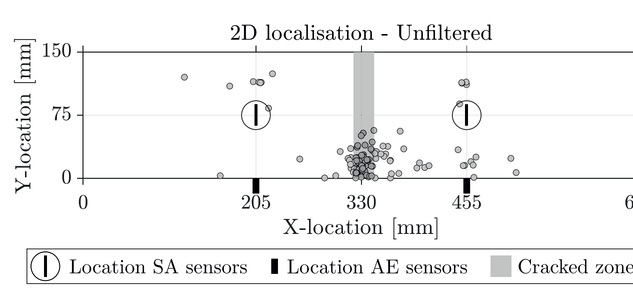

Fig. 11. 2D localization result of prism 1 using an average threshold-based velocity.

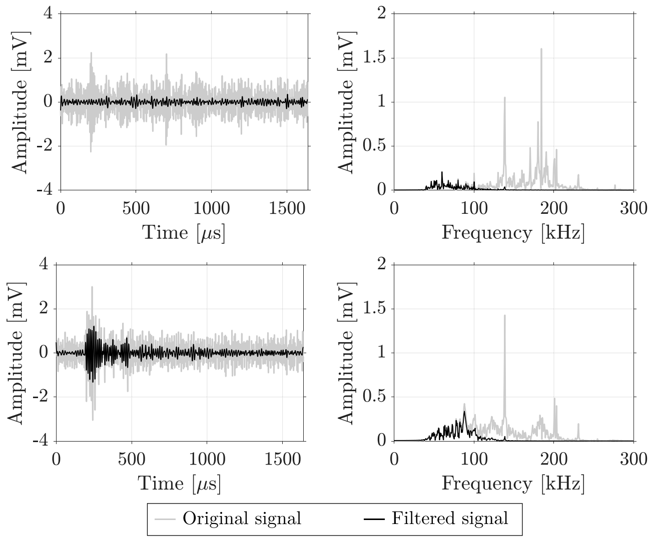

Fig. 12. Unfiltered (grey) and filtered (black) noise signal (top) and signal from concrete cracking (bottom) in time (left) and frequency domain (right).

(SNR) as presented by Van Steen et al. [34], which allows to remove the noise signals. If the SNR was smaller than 10, the signals were removed. Thirdly, the arrival time was determined with the Akaike Information Criterion (AIC) [35,36], instead of threshold-based arrival time picking. For the AE sensors, it was chosen to follow the same procedure in order to obtain similar characteristics to compare the behavior.

After filtering, the average wave velocity is recalculated using the signals captured from pulsing with the AE sensors, and is respectively 2340, 2112, and 2489 m/s for prism 1, prism 2, and prism 3. Note that these values are lower than the threshold-based velocity as the arrival time is based on the filtered waveform of both the pulse and the responses. It was observed that the time difference between pulse and response was higher in case of the filtered signals.

The updated 1D localization result of prism 1 is shown in Fig. 13. After application of the filtering procedure, the AE events are more localized around the middle of the sample where the crack was observed during the three-point bending test, with the SA sensors giving a

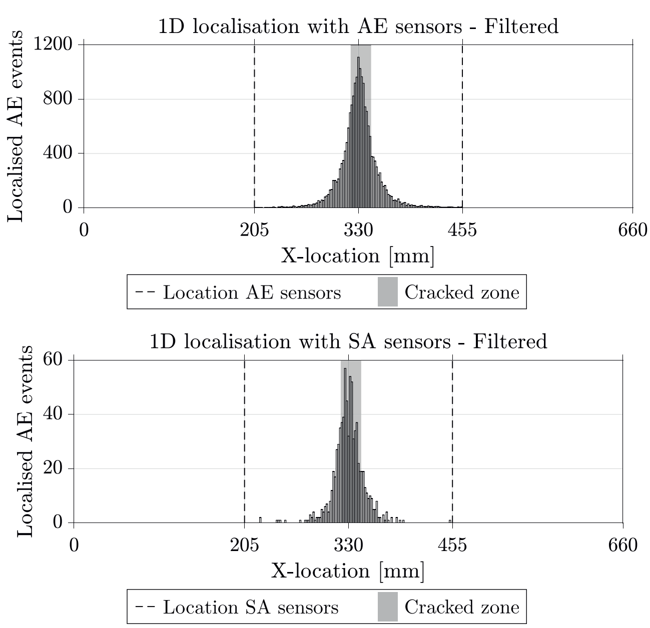

Fig. 13. Updated 1D localization results of prism 1 obtained with the AE sensors (top) and SA sensors (bottom) after filtering.

comparable result as the AE sensors in terms of damage location. It can be seen that the large amount of noise signals located in the middle of the sample is removed. Note that the total amount of captured AE signals is less in case of the SA sensors due to the application of a higher amplitude threshold.

The updated 2D localization result is presented in Fig. 14. Most AE event sources are localized in the region of interest between the sensors, which is the area with a smaller localization error compared to the region outside the sensor array. The events are more distributed along the depth of the sample compared to the threshold-based approach shown in Fig. 11, which confirms the improvement by the analysis procedure.

Fig. 15 shows the AE signals detected by the SA sensor and AE sensor (sensors on the right side of the sample were chosen, see Fig. 5) originating from the same event which was caused by concrete cracking. It can be seen that the peak amplitude values are in the same order of magnitude. In the frequency domain, similar frequencies can be observed with the signal detected by the AE sensor showing slightly lower frequency components compared to the signal detected by the SA sensor. This is of course attributed to a different transfer function of the sensors.

The same analysis procedure was followed for the other two prisms. The 1D and 2D localization results of prism 2 after filtering are shown in Fig. 16. The 2D localization result of prism 3 after filtering is shown in Fig. 17. Again, a good agreement with the experiment is obtained as most events are localized in the middle of the sample where the crack was observed during testing. For prism 2, less events are captured by the SA sensors compared to prism 1 which may be attributed to the installation procedure in voids that were filled with mortar. It can be assumed that this extra interface has an effect on the propagation and attenuation of the AE signal, which is also confirmed by the lower wave velocity found for prism 2.

For prism 3, the sensors layout was different and this alternative arrangement of the sensors leads to an improved 2D localization result. A possibility to further improve the 2D results is to add additional AE sensors at the back of the sample in order that the area of interest is completely surrounded by sensors.

In the previous analysis, qualitative results were presented focusing on whether the SA sensors are able to detect and localize damaged zones. The amplitude threshold for the SA sensors was floating whereas the threshold for the AE sensors was fixed. In order to quantitatively compare the results, the analysis was performed by choosing a fixed and similar threshold for both the SA and AE sensors. This fixed threshold was chosen as the maximum floating threshold found in the respective sample. Fig. 18 shows the 1D localization result of prism 1. Table 4 summarizes the amount of localized AE events for prism 1 and prism 2 with the SA and AE sensors.

In case of prism 1, more events can be localized by the SA sensors compared to the AE sensors as they are placed closer to the damaged zone. However in prism 2, opposite results is obtained. This may be attributed to the core drilling and refilling which may have an important attenuation effect as discussed before.

The results show that SA sensors are successful in the detection and

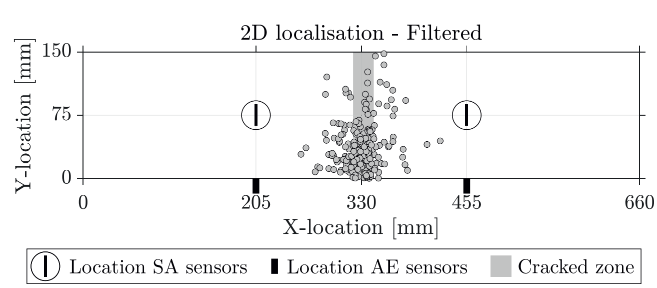

Fig. 14. Updated 2D AE source localization result of prism 1 obtained after filtering.

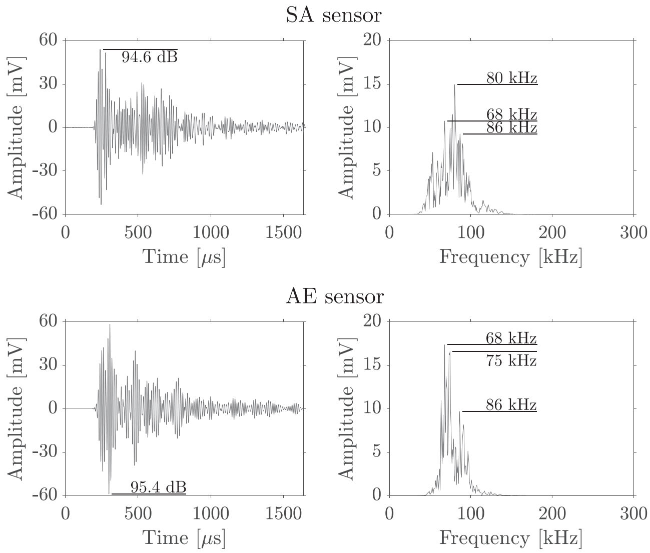

Fig. 15. AE signals in time (left) and frequency (right) domain of the same AE event, with the AE signal, originating from the same event source, detected by SA sensor (top) and AE sensor (bottom).

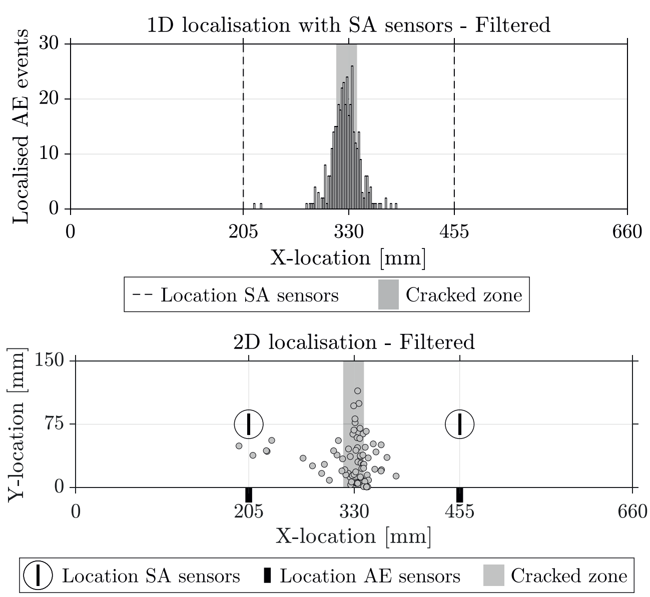

Fig. 16. AE source localization results of prism 2 after filtering of the signals, with 1D (top) and 2D (bottom).

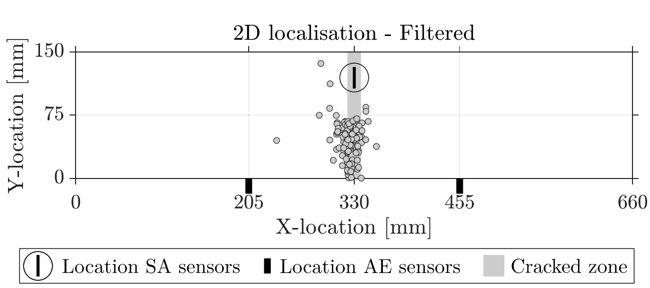

Fig. 17. 2D AE source localization results after filtering of the signals of prism 3.

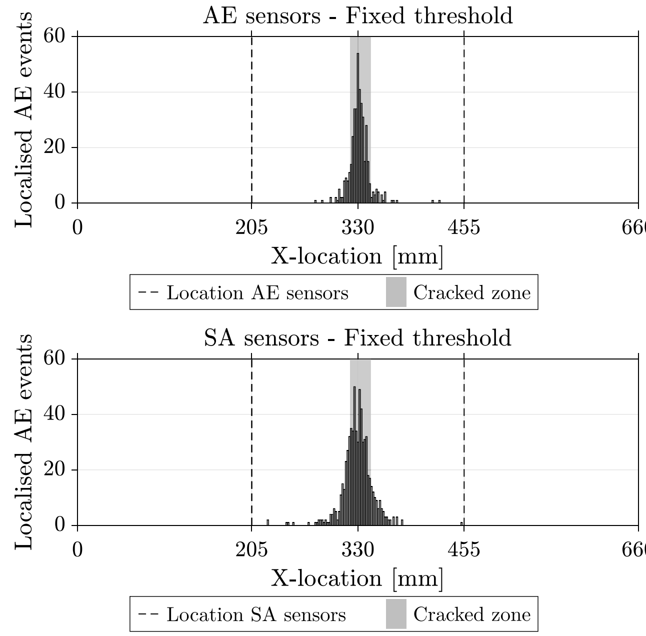

Fig. 18. 1D localization results of prism 1 obtained with the AE sensors (top) and SA sensors (bottom) after filtering and assuming a fixed amplitude threshold for both sensor types.

Table 4
Amount of AE events localized after choosing the same fixed amplitude threshold for all sensors.

Sample name	Fixed threshold [dB]	Amount of AE events localized with	
		AE sensors	SA sensors
Prism 1	68.41	423	698
Prism 2	66.02	641	387

localization of AE signals from concrete cracking during three-point bending tests, although less signals are captured compared to the AE sensors due to the elevated amplitude threshold. Moreover, positioning the SA sensors in a refilled void after core drilling may have an important attenuation effect.

4. Experimental test program: accelerated corrosion test

4.1. Materials and specimen preparation

An RC prism having dimensions 150x150x260 mm was made for the accelerated corrosion test. The concrete composition is shown in Table 5. The mean cube compressive strength was 57.53 MPa (standard deviation 1.43 MPa) as tested on three cubes at 28 days according to EN 12390-3 [30]. The layout of the sample is shown in Fig. 19. The sample was reinforced with a ribbed steel rebar having a diameter of 14 mm. The rebar was placed eccentric resulting in a concrete cover depth of 30 mm. Part of the rebar was coated with anti-corrosive paint and

Table 5
Concrete composition for the sample used in the accelerated corrosion test.

Material	kg/m^3
CEM I 52.5 N	350
Sand 0/4	620
Gravel 4/14	1270
Water	164
Salt	7

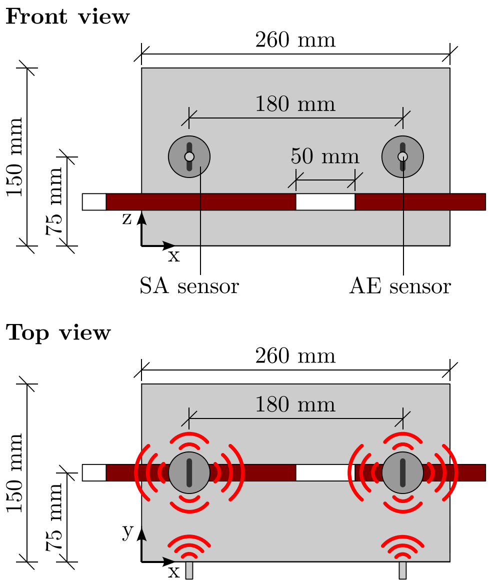

Fig. 19. Front view (top) and top view (bottom) of the RC sample for accelerated corrosion testing with indication of the directionality of the sensors.

covered with a heath shrink wrap to prevent corrosion of these parts (dark red parts in Fig. 19). Only a small section of the rebar (50 mm) was uncoated to allow corrosion. The asymmetric position of the corrosion zone was intentionally designed to ensure that the acquired AE signals are attributed to corrosion and related concrete cracking and to verify that they do not originate from noise which would be localized in the middle, as discussed in previous section. Fig. 20 shows a picture of the formwork and SA before concrete casting. The SA sensors were placed in the middle of the height of the sample with a horizontal distance of 180 mm in between.

4.2. Acoustic emission sensing

The specimen was continuously monitored during the accelerated corrosion test with the AE technique. Besides the two SA sensors that were embedded in the concrete, two AE sensors were attached on the surface with vacuum grease. The horizontal distance between the sensors was 180 mm, see Fig. 19. The same sensor type and specifications were used as during the three-point bending tests. The coordinates of the sensors are listed in Table 6.

4.3. Accelerated corrosion test

The corrosion process was accelerated by use of a power supply with a direct current. The positive side was connected to the rebar and the negative side to a stainless-steel plate. The sample was partially submerged in a 5 % sodium chloride solution and salt was pre-mixed in the concrete (see composition in Table 5). A current density of 50 μA/cm^2 was applied. A schematic view of the setup is shown in Fig. 21. The

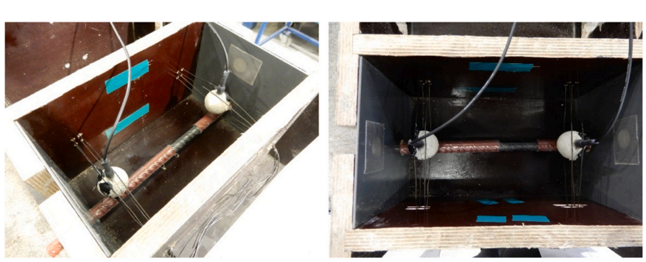

Fig. 20. Pictures of the formwork of the sample for the accelerated corrosion test.

Table 6
Coordinates of the SA and AE sensors during the accelerated corrosion test.

	X [mm]	Y [mm]	Z [mm]
SA 1	40	75	75
SA 2	220	75	75
AE 1	40	0	75
AE 2	220	0	75

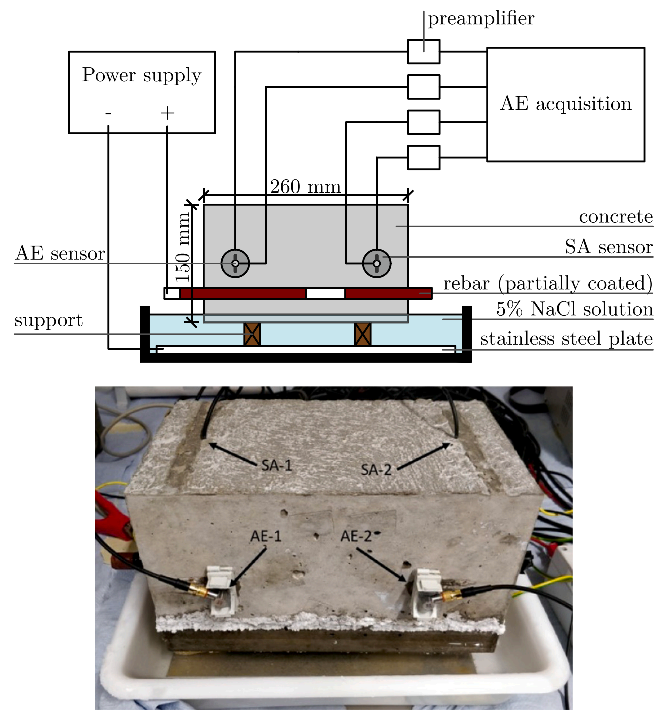

Fig. 21. Schematic representation (top) and picture (bottom) of the accelerated corrosion setup.

corrosion crack width on the concrete surface was measured at 5 different positions every 3 days with DEMEC points with a distance of 10 cm between each other.

4.4. Results of the accelerated corrosion test and discussion

Similar to the three-point bending tests, many noise signals were detected during the accelerated corrosion test. The noise signals have peak frequencies around 50 and 100 kHz (Fig. 22). An example of such a signal is shown in Fig. 23. Therefore, a high pass Butterworth filter of order 10 with a cut-off frequency of 125 kHz and a lowpass Butterworth filter of order 10 with a cut-off frequency of 180 kHz were applied to reduce the noise level. The same filter was applied to the AE signals

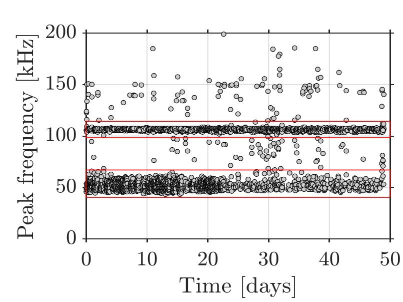

Fig. 22. Peak frequency versus time of the AE signals captured with the SA sensors. Noisy signals are clustered around 50 and 100 kHz as indicated in red.

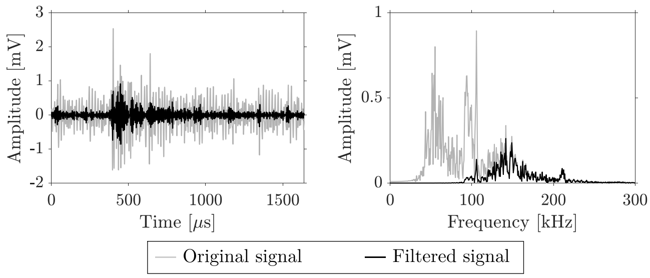

Fig. 23. Unfiltered (grey) and filtered (black) signal in time (left) and frequency domain (right).

captured by the surface-bonded AE sensors.

The wave velocity was determined by pulsing from the AE sensors to the other sensors. A threshold-based velocity of 4080 m/s was obtained. This value was adapted after filtering (Butterworth filter and AIC picker) to 3330 m/s.

The 1D localization result of the AE and SA sensors obtained with a threshold-based velocity and without filtering is shown in Fig. 24. For the AE sensors, it can be observed that most AE signals are localized within the corrosion zone and at the location of the corrosion-induced crack. For the SA sensors, most events are localized in the middle of the sample, which is an indication of noise.

The localization result after filtering is shown in Fig. 25. Here, the evolution of the localized events over time is shown as well as the evolution of the crack width. It can be seen that most AE signals are

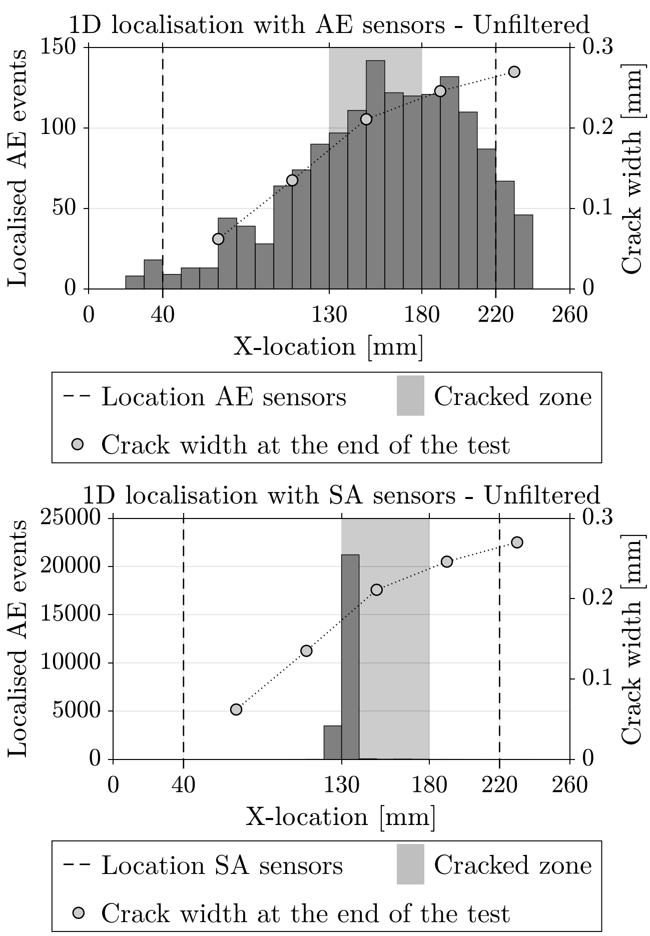

Fig. 24. 1D localization results using an average threshold-based velocity, obtained with AE sensors (left) and SA sensors (right) with indication of the crack width at the end of the test.

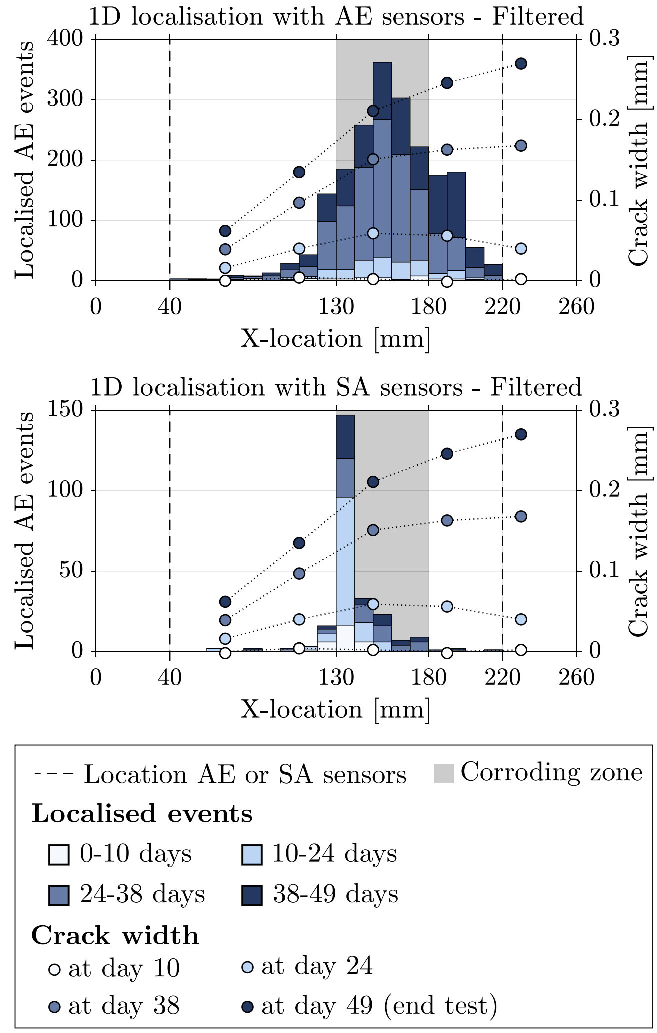

Fig. 25. Updated 1D localization results obtained with AE sensors (left) and SA sensors (right) after filtering with indication of the crack width.

localized within the asymmetric corrosion zone for both the AE and SA sensors. For the SA sensors, comparatively more AE signals were localized early in the corrosion process, which is between the start of the test and 24 days. For the AE sensors, a larger share of the signals was localized in a later stage of the test when larger crack widths were observed on the sample surface. This may indicate that SA sensors are more sensitive to corrosion signals, which are characterized by a lower amplitude and energy, compared to surface-bound AE sensors that are more sensitive to concrete cracking. This observation is promising for early-age corrosion damage detection with SA sensors.

Following the analysis procedure of the three-point bending tests, the amount of localized AE events was investigated after assuming a fixed and similar amplitude threshold for both sensor types. A fixed threshold of 70 dB was chosen as this was the maximum floating threshold for the SA sensors.

Fig. 26 shows the 1D localization result for the AE sensors (left) and the SA sensors (right). It can be observed that less events were localized when only using the AE sensors (18 events). Moreover, the events are mainly detected during concrete cover cracking. As mentioned before, signals related to corrosion showed a lower amplitude and are therefore not exceeding the fixed amplitude threshold. SA sensors are able to detect more events (201 events). Events can be localized from the beginning of the test, proving that the sensors are more sensitive to corrosion signals.

Fig. 27 shows the 2D localization result after filtering with indication

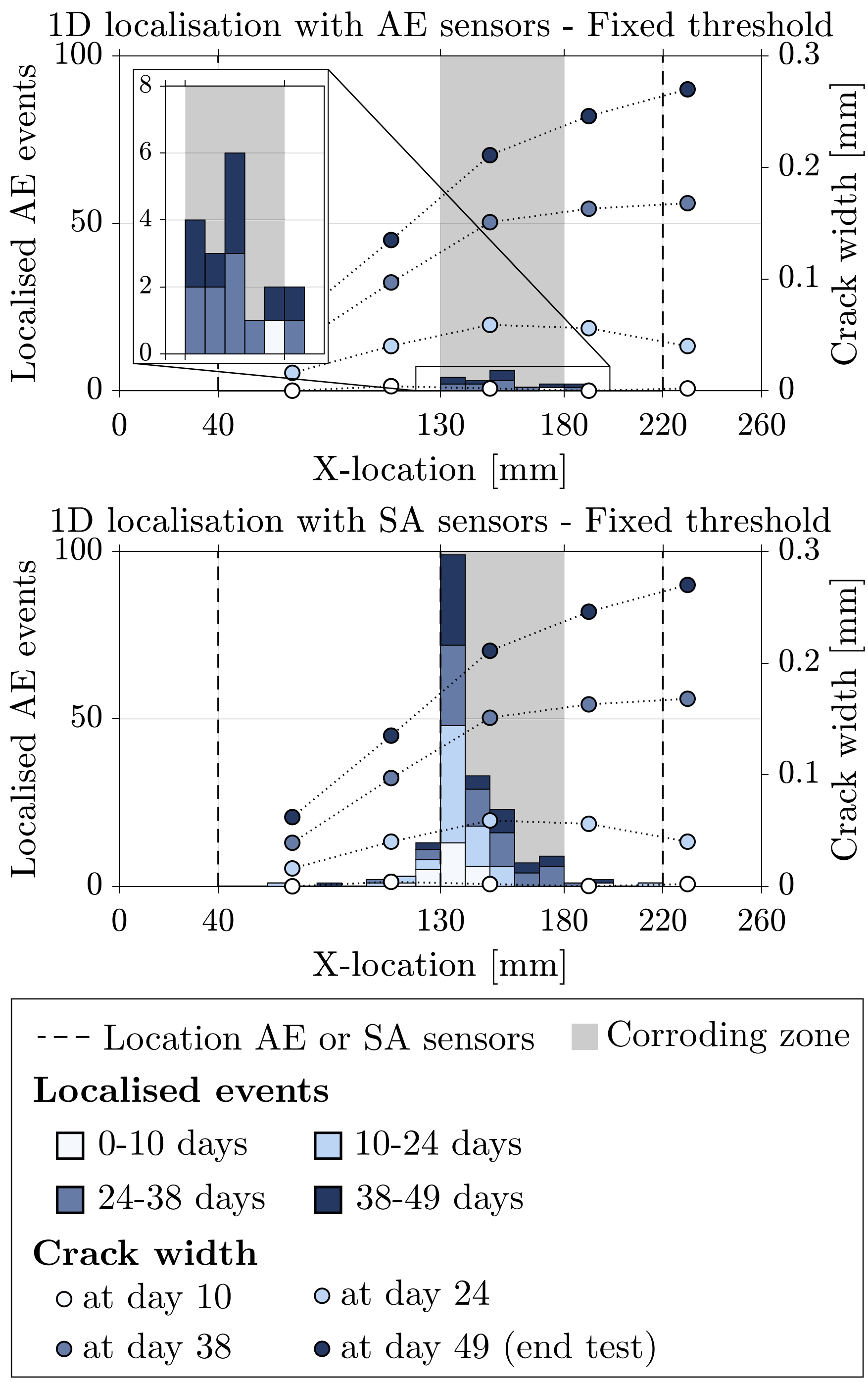

Fig. 26. 1D localization results obtained with the AE sensors (left) and SA sensors (right) after filtering and assuming a fixed amplitude threshold for both sensor types.

of the location of the AE and SA sensors and the observed corrosion-induced crack, as well as a picture of the cracked surface. For the 2D localization results, both sensor types (embedded sensors (SA) and surface-mounted AE sensors) were combined. Only few AE events could be localized in 2D. However, all AE events are located around the corroding zone. As mentioned before in Section 3, most AE events are localized within the sensor array, which is less prone to errors. However, in the current setup, both AE and SA sensors are positioned in a plane that is 31 mm above the corroding rebar and the corrosion cracks grow towards the bottom, away from this plane. As a next step for further research, the feasibility of 2D or 3D localization with SA sensors may be interesting to investigate when considering an optimized sensor placement serving this purpose.

Overall, less AE signals could be localized during the accelerated corrosion test than during the three-point bending tests. During the accelerated corrosion test, AE signals had a lower amplitude compared to AE signals obtained during the three-point bending test. Due to the high noise level of the SA sensors, AE signals with a low amplitude could not be captured. Yet, the results show that SA sensors are well capable of detecting AE signals originating from rebar corrosion and corrosion-induced cracking.

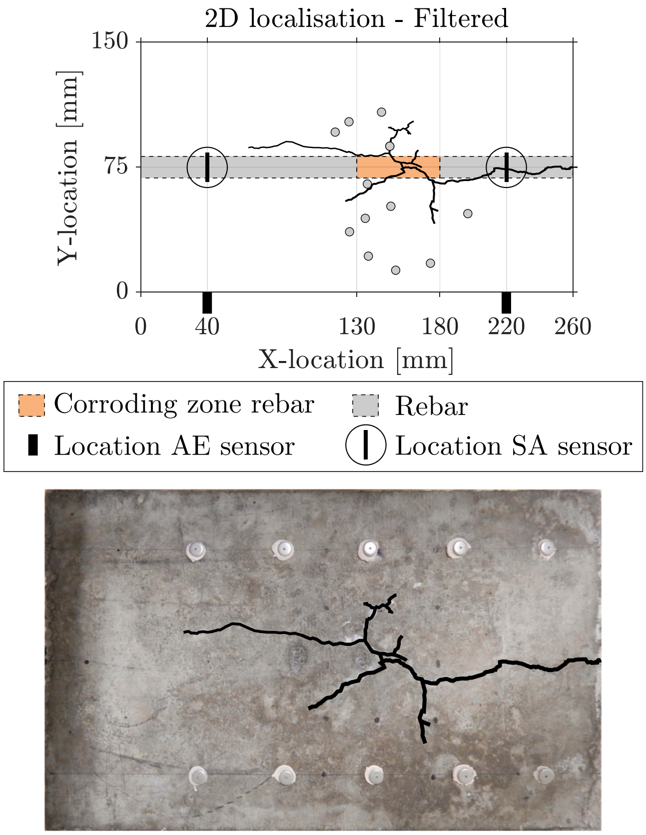

Fig. 27. 2D localization result after filtering with indication of the corroding zone and cracking pattern (top) and picture of the cracked sample after the corrosion test with indication of the crack pattern (bottom). Note that the crack is exaggerated for clearness.

5. Discussion on the use of embedded sensors for acoustic emission monitoring of concrete structures

From the presented results it can be seen that embedded sensors (or SA sensors) are promising to serve as an alternative or addition to surface-mounted AE sensors in terms of damage detection and localization. Moreover, SA sensors may provide useful advantages over surface-mounted sensors. Embedded sensors are protected from the environment and thus external damage, leading to potentially longer operational life and consistent performance. This makes them suitable for long-term monitoring. As they can be positioned closer to the AE source, embedded sensors can detect signals with less attenuation and interference along the wave's travel path, resulting in higher sensitivity and accuracy. However, embedded sensors have their limitations as well. The installation of embedded sensors can be challenging and costly. They can be embedded before concrete casting by attaching them to the reinforcement or afterwards by embedding while refilling a void after core drilling. Once embedded, these sensors are difficult to access for maintenance, repair, or replacement. Also their position is fixed and cannot be changed after installation. Considering these advantages and disadvantages, the choice for embedded sensors, surface-mounted sensors, or a combination of both depends on the monitoring application, including accessibility, budget, environmental conditions, and requirements for signal sensitivity and accuracy.

6. Conclusions

This paper investigated the feasibility to use smart aggregates for passive AE monitoring of cracking and rebar corrosion in (reinforced) concrete. Cracking was induced by means of three-point bending tests and by reinforcement corrosion. The tests induce a different cracking behavior and crack orientation.

The results showed a relatively high noise level for the SA sensors, which masked part of the cracking signals and adversely affected the localization process. It was observed that more AE signals could be localized during the three-point bending tests than during the corrosion test. AE signals with a higher amplitude are captured during three-point bending tests compared to the corrosion test.

After dedicated filtering to counter the high noise level, SA sensors are able to detect concrete cracking during both tests. 1D AE localization results obtained with the SA sensors are comparable to the result of the AE sensors. AE signals captured by both AE and SA sensors could be localized in 2D, and most AE signals are located within the cracked zone of the samples. It can be concluded that SA sensors are promising to serve as an alternative or addition to classic AE sensors in terms of damage detection and localization. Moreover, the SA sensors seem to provide higher sensitivity in measuring rebar corrosion compared to the conventional surface-bonded sensors. This offers potential for early-stage corrosion damage in reinforced concrete structures.

Still, the high noise level remains an important challenge. Therefore, future work will focus on the sensitivity of the SA sensors and a reduction of the noise level.

CRediT authorship contribution statement

Charlotte Van Steen: Writing – review & editing, Writing – original draft, Visualization, Validation, Software, Methodology, Investigation, Funding acquisition, Formal analysis, Data curation, Conceptualization. **Lotfollah Pahlavan:** Writing – review & editing, Writing – original draft, Supervision, Resources, Conceptualization. **Els Verstrynge:** Writing – review & editing, Writing – original draft, Supervision, Funding acquisition, Conceptualization.

Declaration of Competing Interest

The authors declare that they have no known competing financial interests or personal relationships that could have appeared to influence the work reported in this paper.

Data availability

Data will be made available on request.

Acknowledgements

The authors gratefully acknowledge SHM NEXT for providing the smart aggregates for the experimental tests. The financial support by FWO-Flanders for the Postdoctoral Mandate of C. Van Steen (Grant No. 12ZD221N) is gratefully acknowledged.

References

[1] A. Carpinteri, A. Grazzini, G. Lacidogna, A. Manuello, Durability evaluation of reinforced masonry by fatigue tests and acoustic emission technique, Struct. Control Health Monit. 21 (2014) 950–961.
[2] G. Manthei, Characterization of acoustic emission sources in a rock salt specimen under triaxial compression, Bull. Seismol. Soc. Am. 95 (5) (2005) 1674–1700.
[3] A. Marec, J.-H. Thomas, R. El Guerjouma, Damage characterization of polymer-based composite materials: multivariable analysis and wavelet transform for clustering acoustic emission data, Mech. Syst. Signal Process. 22 (2008) 1441–1464.
[4] A.K. Tomor, E. Verstrynge, A joint fatigue–creep deterioration model for masonry with acoustic emission based damage assessment, Constr. Build. Mater. 43 (2013) 575–588.
[5] A. Behnia, H.K. Chai, T. Shiotani, Advanced structural health monitoring of concrete structures with the aid of acoustic emission, Constr. Build. Mater. 65 (2014) 282–302.
[6] M. De Smedt, R. Vrijdaghs, C. Van Steen, E. Verstrynge, L. Vandewalle, Damage analysis in steel fibre reinforced concrete under monotonic and cyclic bending by means of acoustic emission monitoring, Cem. Concr. Compos. 114 (2020) 103765.

[7] R. Kravchuk, E.N. Landis, Acoustic emission-based classification of energy dissipation mechanisms during fracture of fiber-reinforced ultra-high performance concrete, Constr. Build. Mater. 176 (2018) 531–538.
[8] K. Ohno, K. Uji, A. Ueno, M. Ohtsu, Fracture process zone in notched concrete beam under three-point bending by acoustic emission, Constr. Build. Mater. 67 (part B) (2014) 139–145.
[9] E. Selman, A. Ghiami, N. Alver, Study of fracture evolution in FRP-strengthened reinforced concrete beam under cyclic load by acoustic emission technique: an integrated mechanical-acoustic energy approach, Constr. Build. Mater. 95 (2015) 832–841.
[10] C. Van Steen, E. Verstrynge, M. Wevers, L. Vandewalle, Assessing the bond behaviour of corroded smooth and ribbed rebars with acoustic emission monitoring, Cem. Concr. Res. 120 (2019) 176–186.
[11] A. Gallego, A. Benavent-Climent, E. Suarez, Concrete-galvanized steel pull-out bond assessed by acoustic emission, J. Mater. Civ. Eng. 28 (2) (2016) 04015109.
[12] W. Lei, Y. Jin, X. Hailong, F. Lei, Experimental study of a pull-out test of corroded steel and concrete using acoustic emission monitoring method, Constr. Build. Mater. 122 (2016) 163–170.
[13] C. Van Steen, H. Nasser, E. Verstrynge, M. Wevers, Acoustic emission source characterisation of chloride-induced corrosion damage in reinforced concrete, Struct. Health Monit. 21 (3) (2022) 1266–1286.
[14] Y. Kawasaki, T. Wakuda, T. Kobarai, M. Ohtsu, Corrosion mechanisms in reinforced concrete by acoustic emission, Constr. Build. Mater. 48 (2013) 1240–1247.
[15] M. Ohtsu, K. Mori, Y. Kawasaki, Corrosion process and mechanisms of corrosion-induced cracks in reinforced concrete identified by AE analysis, Strain 47 (2) (2011) 179–186.
[16] E. Verstrynge, C. Van Steen, E. Vandecruys, M. Wevers, Steel corrosion damage monitoring in reinforced concrete structures with the acoustic emission technique: a review, Constr. Build. Mater. 349 (2022) 128732.
[17] Y. Farnam, M.R. Geiker, D. Bentz, J. Weiss, Acoustic emission waveform characterization of crack origin and mode in fractured and ASR damaged concrete, Cem. Concr. Compos. 60 (2015) 135–145.
[18] M. Abdelrahman, M.K. ElBatanouny, P. Ziehl, J. Fasl, C.J. Larosche, J. Fraczek, Classification of alkali-silica reaction damage using acoustic emission: a proof-of-concept study, Constr. Build. Mater. 95 (2015) 406–413.
[19] S. Zhao, S. Fan, J. Yang, S. Kitipornchai, A spherical smart aggregate sensor based electro-mechanical impedance method for quantitative damage evaluation of concrete, Struct. Health Monit. 19 (5) (2020) 1560–1576.
[20] Grosse, C.U., Ohtsu, M., Aggelis, D.G., and Shiotani, T., eds. Acoustic Emission Testing - Basics for Research - Applications in Engineering. 2021, Springer.
[21] H. Gu, G. Song, H. Dhonde, Y.L. Mo, S. Yan, Concrete early-age strength monitoring using embedded piezoelectric transducers, Smart Mater. Struct. 15 (2006) 1837–1845.
[22] G. Song, H. Gu, Y.-L. Mo, Smart aggregates: multi-functional sensors for concrete structures - a tutorial and a review, Smart Mater. Struct. 17 (2008) 033001.
[23] Y. Moslehy, H. Gu, A. Belarbi, Y.L. Mo, G. Song, Smart Aggregate-Based Damage Detection of Circular RC columns under Cyclic Combined Loading, Smart Mater. Struct. 19 (6) (2010) 065021.
[24] C. Dumoulin, G. Karaiskos, A. Deraemaeker, Monitoring of crack propagation in reinforced concrete beams using embedded piezoelectric transducers. Woodhead Publishing Series in Civil and Structural Engineering, Acoust. Emiss. Relat. Non-Destr. Eval. Tech. Fract. Mech. Concr. *8* (2015) 161–175.
[25] P. Liu, Y. Hu, B. Geng, D. Xu, Corrosion monitoring of the reinforced concrrete by using the embedded annular piezoelectric transducer. J. Mater. Res. Technol. 9 (3) (2020) 3511–3519.
[26] W. Li, Q. Kong, S.C.M. Ho, I. Lim, Y.L. Mo, G. Song, Feasibility study of using smart aggregates as embedded acoustic emission sensors for health monitoring of concrete structures, Smart Mater. Struct. 25 (2016) 115031.
[27] European Committee for Standardization, EN 1330-9: Non-destructive testing - Terminology - Part 9: Terms used in acoustic emission testing. 2017.
[28] Y. Lu, J. Zhang, Z. Li, B. Dong, Corrosion monitoring of reinforced concrete beam using embedded cement-based piezoelectric sensor, Mag. Concr. Res. 65 (21) (2013) 1265–1276.
[29] European Committee for Standardization, EN 14651: Test method for metallic fiber concrete - measuring the flexural tensile strength (limit of proportionality (LOP), residual). 2014.
[30] European Committee for Standardization, EN 12390-3: Testing hardened concrete - Part 3: Compressive strength of test specimens. 2019.
[31] European Committee for Standardization, EN196-1: Methods of testing cement - Part 1: Determination of strength. 2016.
[32] Vallen Systeme, The Vallen AE-Suite software Help. 2016.
[33] M. Ge, Analysis of source location algorithms, Part II: iterative methods, J. Acoust. Emiss. 21 (2003) 29–51.
[34] C. Van Steen, E. Verstrynge, Degradation monitoring in reinforced concrete with 3D localization of rebar corrosion and related concrete cracking, Appl. Sci. 11 (15) (2021) 6772.
[35] H. Akaike, Markovian representation of stochastic processes and its application to the analysis of autoregressive moving average processes, Ann. Inst. Stat. Math. 26 (1) (1974) 363–387.
[36] J.H. Kurz, C.U. Grosse, H.W. Reinhardt, Strategies for reliable automatic onset time picking of acoustic emissions and ultrasound signals in concrete, Ultrasonics 43 (2005) 538–546.